The crystal structure of the superconductor $HgBa_2Ca_2Cu_3O_{8+\delta}$ with Pb substitution

1997 J. Phys.: Condens. Matter 9 1451

(http://iopscience.iop.org/0953-8984/9/7/010)

J. Phys.: Condens. Matter **9** (1997) 1451–1460. Printed in the UK PII: S0953-8984(97)76782-1

The crystal structure of the superconductor $HgBa_2Ca_2Cu_3O_{8+\delta}$ with Pb substitution

X S Wu†, S S Jiang†, H M Shao†, F M Pan†, N Xu†, Mao Zhiqing‡, Zuo Jian‡ and Zhang Yuheng‡

† National Laboratory of Solid State Microstructures, Institute of Solid State, and Centre for Advanced Studies in Science and Technology of Microstructures, Nanjing University, Nanjing 210093, People's Republic of China

‡ Structure Research Laboratory, University of Science and Technology of China, Heifei, Anhui 230026, People's Republic of China

Received 31 July 1996, in final form 20 December 1996

Abstract. Pb-doped $Hg_{1-x}Pb_xBa_2Ca_2Cu_3O_{8+\delta}$ superconductors with $x = 0.0$ to 0.50 and increment steps of 0.1 have been synthesized. For $x = 0.30$, the sample has the highest superconducting transition temperature, $T_c^{R=0} = 135$ K (the zero-resistance temperature), and $T_c^{\text{onset}} = 143$ K (the diamagnetic onset temperature) (results given by Shao H M, Lam C C, Fung P C W, Wu X S, Du J H, Shen G J, Chow J C L, Ho S L, Hung K C and Yao X X 1995 *Physica* C **246** 207). The crystal structures of these solid solutions have been investigated by synchrotron x-ray diffraction (SXRD) and Raman spectroscopy at room temperature. The lattice parameters decrease with the increase of the content of Pb. From SXRD refinements, one of the most significant features of this study is that there are great differences between some of the cation–oxygen bond distances—such as the (Hg/Pb)–O bond distance—of Pb-free and Pb-doped samples. The impurity phases appearing in our samples are $CaHgO_2$ and $BaCuO_2$, which are refined together. The content of each phase is determined from the refined scale factor. Raman studies show that the peaks appearing at 232 cm^{-1}, 671 cm^{-1}, and 632 cm^{-1} are due to the impurity phase, and four peaks at the frequencies of 107 cm^{-1}, 477 cm^{-1}, 577 cm^{-1} and 597 cm^{-1} are due to the vibrations of oxygen atoms in the superconducting phase. No Raman peak shift is observed when the laser irradiation power is changed.

1. Introduction

Since the discovery of superconductivity in the mercury-based cuprates [1, 2], three phases bearing the formula $HgBa_2Ca_{n-1}Cu_nO_{2n+2+\delta}$ (Hg-12$(n-1)n$), where $n = 1$, 2, 3, have been isolated [3–5]. The 1223 phase $HgBa_2Ca_2Cu_3O_{8+\delta}$ (Hg-1223; $n = 3$) has a T_c of about 135 K under atmospheric pressure and it can even achieve a critical temperature of $T_c = 164$ K under high pressure [6]. The structures of these mercury-based cuprates have been widely studied by x-ray diffraction, neutron powder diffraction and Raman measurements [7–15]. The crystal structure of this mercury-based compound has a space group symmetry of $P4/mmm$, which is similar to the crystal structures of the Tl-based compounds $Tl(Ba, Sr)_2Ca_2Cu_3O_{8+\delta}$. The main difference between the crystal structures of these two types of compound lies in the amount of oxygen deficiency in the Hg–O plane as compared to that in the Tl–O plane. The former is less than 50%, and the latter almost 1.0. The structure of Hg-1223 (shown in figure 1) is based on the layer sequence

$$\cdots(CuO_2)(Ca)(CuO_2)(BaO)(HgO_\delta)(BaO)(CuO_2)(Ca)(CuO_2)\cdots$$

0953-8984/97/071451+10$19.50

in which rock-salt blocks of $(BaO)(HgO_\delta)(BaO)$ alternate with oxygen-deficient perovskite-like $(CuO_2)(Ca)(CuO_2)$ blocks.

Recently, there have been several attempts [16–20] to synthesize new Hg-based compounds using substitution. For example, Isawa *et al* [16] have studied the effect of Pb doping in Hg-1223 with contents of Pb up to 20%, and found that it decreased T_c. Hur *et al* [17] found that Hg-based $Hg_{0.5}Tl_{0.5}Ba_2(Ca_{0.86}Sr_{0.14})_2Cu_3O_{8+\delta}$ had a T_c of 132 K, less than that of the pure Hg-1223 compound. However, Dai *et al* [18] and Shao *et al* [19] have successfully synthesized Tl-doped $Hg_{0.8}Tl_{0.2}Ba_2Ca_2Cu_3O_{8+\delta}$ and Pb-doped $Hg_{0.7}Pb_{0.3}Ba_2Ca_2Cu_3O_{8+\delta}$ superconductors, respectively. They found that the critical temperatures of the Tl- and Pb-doped Hg-1223 superconductors could reach 138 K (zero-resistance temperature) and 135 K (zero-resistance temperature), respectively. These results indicate that the superconducting transition temperature of the material with substitution can be enhanced. The structure of Tl-doped Hg-1223 superconductor has been determined by neutron powder diffraction [18]. A neutron powder diffraction investigation has also been carried out on Pb-doped $Hg_{0.7}Pb_{0.3}Ba_2Ca_2Cu_3O_{8+\delta}$. Here, we carry out Pb-substitution experiments on the Hg-1223 compound. Synchrotron x-ray diffraction measurements are carried out on $Hg_{1-x}Pb_xBa_2Ca_2Cu_3O_{8+\delta}$ samples at room temperature. Raman spectra of $Hg_{0.7}Pb_{0.3}Ba_2Ca_2Cu_3O_{8+\delta}$ ($x = 0.30$) for different laser irradiation powers are obtained. The results of these studies are reported herein.

2. Experimental details

The powder samples of $Hg_{1-x}Pb_xBa_2Ca_2Cu_3O_{8+\delta}$ were synthesized as described elsewhere [19, 21]. Briefly, a nominal $Ba_2Ca_2Cu_3O_7$ precursor is prepared firstly. Powders of HgO (99.9%) and PbO (99.9%) are mixed with the precursor and ground. The cation ratio of $Hg_{1-x}Pb_x$/Ba/Ca/Cu is 1/2/2/3, where x varies from 0.0 to 0.5 in steps of 0.1. The ground powder is then pressed into pellets with rectangular dimensions of $2 \times 4 \times 20$ mm^3. The pressed pellets are sealed together in a vacuum tube. The rapid-annealing technique is repeated four times as described in reference [19]. To prevent the sputtering of the quartz lining and production of mercury fragments due to possible explosions, this tube is placed in a steel container. The whole system is put into a furnace and slowly heated to a temperature of 850 °C (at a rate of $\sim$4 °C min^{-1}). This temperature is maintained for ten hours. Then the system is cooled to 200 °C at the same rate as for the heating process. The samples are maintained at this temperature for two hours. Finally the whole system is cooled to room temperature in the furnace. After sintering, some of the samples are annealed in O_2 at 240 °C for ten hours. Then the samples are cooled to room temperature in air or in the furnace. The calcined samples are immediately put into a desiccator for further measurements.

The synchrotron x-ray diffraction (SXRD) investigation was carried out at room temperature at the diffraction station at Beijing Synchrotron Radiation Laboratory (BSRL) for the Hg-1223 and Pb-doped samples. The wavelength used in our experiment was 1.5401 Å. The step-scan diffraction data were collected over the angular range of $4^\circ \leqslant 2\theta \leqslant 80^\circ$. A 2θ-step size of 0.02° and a counting time of 5 s per point were used. Structural characterization of the pure and Pb-doped Hg-1223 superconductors for the neutron powder diffraction data and the SXRD data were carried out by Rietveld profile analysis with the RIETAN software package [22].

The 'R-factors' and the 'goodness of fit' are used as the numerical criteria of the fit. The definitions of the 'R-factors' and the 'goodness of fit' are as follows:

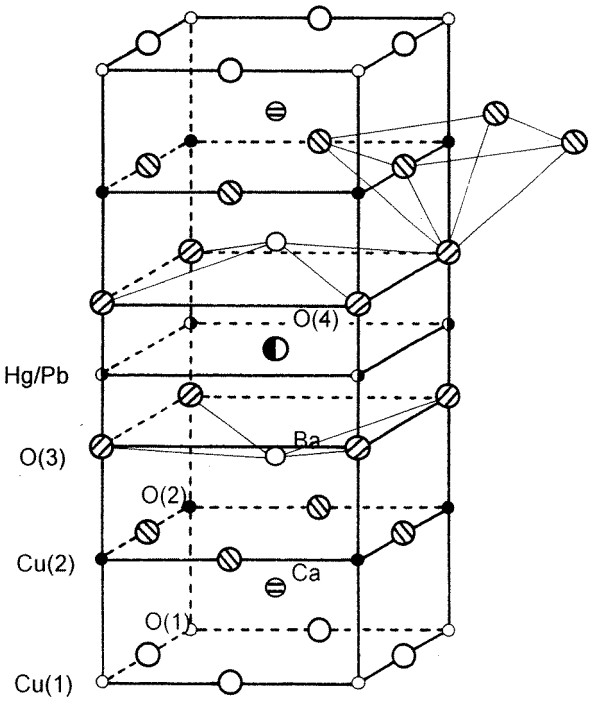

Figure 1. A schematic representation of the structure of (Hg, Pb)$Ba_2Ca_2Cu_3O_{8+\delta}$.

(i) the pattern R-factor:

$$R_p = \sum_{i=1}^{N} |Y_{oi} - Y_{ci}| \Big/ \sum_{i=1}^{N} |Y_{oi}|$$

(ii) the weighted pattern R-factor:

$$R_{wp} = \left\{ \sum_{i=1}^{N} w_i (|Y_{oi} - Y_{ci}|)^2 \Big/ \sum_{i=1}^{N} |Y_{oi}|^2 \right\}^{1/2}$$

(iii) the expected R-factor:

$$R_{exp} = \left\{ (N - P + C) \Big/ \sum_{i=1}^{N} w_i |Y_{oi}| \right\}^{1/2}$$

(iv) the 'goodness of fit':

$$S = \frac{R_{wp}}{R_{exp}}$$

where Y_{oi}, Y_{ci} are the observed and calculated intensities at the ith step, respectively, w_i is the weight ($=1/Y_{oi}$), N is the total number of points, P is the adjusted parameter, and C is the number of constraints applied. For all systems refined, some refined 'R-factors', such as R_p, R_{exp}, and R_{wp}, are given in table 2. These 'R-factors' indicate that the refinement is good.

The background is refined. According to RIETAN, the background intensity at the ith step, Y_{ib}, can be refined from a refinable background function:

$$Y_{ib} = b_0 + b_1 Z_i + b_2 Z_i^2 + b_3 Z_i^3 + b_4 Z_i^4 + b_5 Z_i^5$$
$$Z_i = \frac{2\theta_i - \theta_{max} - \theta_{min}}{\theta_{max} - \theta_{min}}.$$

The background parameters b_0–b_5 are refined periodically during the refinement process. The FWHM parameters for each phase are refined and set as the same. To ensure that our refinements reach a stable convergence, the refinement is performed according to the following group order:

(1) scale factors/background function/zero-point shift;
(2) cell parameters;
(3) peak shape/half-width/asymmetry parameter/preferred orientation;
(4) atomic position parameter;
(5) site occupancies;
(6) overall thermal parameters;
(7) isotropic thermal parameters.

Raman measurements are made on Pb-free and Pb-doped ($x = 0.30$) samples at room temperature using a 5PEX-1403 in a back-scattering geometry. The spectra are excited with the 5145 Å line (green) of an argon-ion laser focused on the freshly exposed surfaces of the samples. The sampling area is several μm^2. The detector is a silicon diode array. Usually, a spectrum is obtained by accumulating about 100 measurements with an acquisition time of 5 s each.

Superconducting properties are characterized by resistance and magnetic susceptibility measurements. The standard four-probe technique is used to determine the resistances of the samples. AC magnetic susceptibility measurements are also carried out using the mutual-inductance technique with an AC signal of 160 Hz and magnetic field amplitude of $H_m = 0.2$ Oe.

Table 1. The calculated lattice parameters (tetragonal structure, a and c in Å) for as-prepared $(Hg_{1-x}Pb_x)$-1223 samples.

x	0.0	0.1	0.2	0.3	0.4	0.5
a	3.8546(4)	3.8499(6)	3.8478(2)	3.8428(3)	3.8417(1)	3.8398(2)
c	15.8424(5)	15.8357(3)	15.8306(7)	15.8237(5)	15.8180(8)	15.8217(9)

3. Results and discussion

The lattice parameters for the as-prepared samples are characterized by SXRD and are calculated using the least-squares method. The impurity phase reflections are removed during the calculation. The fitted values are listed in table 1. The a-axis and c-axis lattice parameters decrease with the increase of the content of Pb, x. This result indicates that Pb can replace Hg to form an (Hg, Pb)-1223 solid solution with up to 50% of Pb. On the other hand, the observed critical temperature [19] T_c of the as-prepared samples varies strongly with x, increasing from 110 K for $x = 0.0$ to a maximum of $T_c = 130$ K at $x = 0.30$, and then decreasing with x, for larger x. The relation between the a-axis lattice parameter and T_c is similar to that for pure mercury-based homologous series superconductors [7].

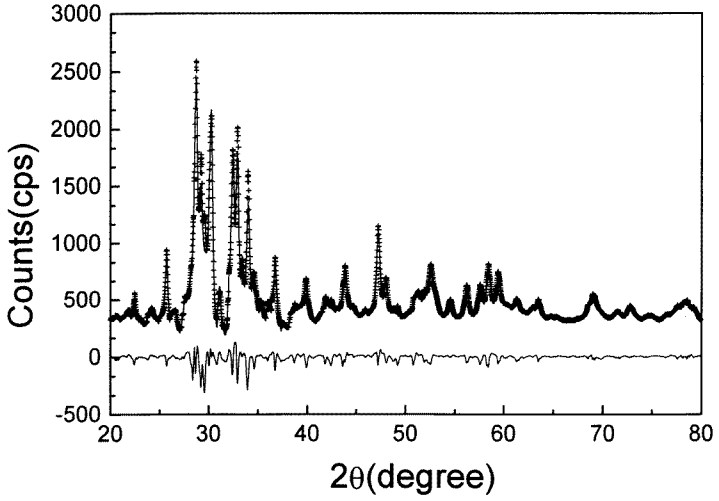

Figure 2. Measured and calculated x-ray diffraction intensities (+ and continuous line, respectively) for the sample of $Hg_{0.7}Pb_{0.3}Ba_2Ca_2Cu_3O_{8.46}$ at room temperature. The difference curve (observed − calculated values) is also shown at the bottom of the figure.

The x-ray diffraction patterns for each of the oxygenated $Hg_{1-x}Pb_xBa_2Ca_2Cu_3O_{8+\delta}$ cuprates show that our sample does contain impurity phases like $BaCuO_2$ and $CaHgO_2$. However, our samples are essentially single phase—that is, samples for which measurements are made in this work do not contain any other superconducting phases like Hg-1201 and Hg-1212. Hence, the x-ray diffraction and neutron powder diffraction data are analysed using Izumi's Rietveld structure refinement program RIETAN [22]. This program can handle a mixture of two or more phases. We assume that the Pb-doped sample has the same symmetry as the Pb-free sample. The results obtained by Chmaissem *et al* [8] are used as an initial model for our Pb-free and Pb-doped Hg-1223 samples. The initial lattice constants and atomic coordinates for the $CaHgO_2$ and $BaCuO_2$ phases are taken from references [9] and [23], respectively. The refined results for $HgBa_2Ca_2Cu_3O_{8+\delta}$ (SXRD) and for $Hg_{0.7}Pb_{0.3}Ba_2Ca_2Cu_3O_{8+\delta}$ (SXRD and NPD [20]) are summarized in table 1. Figure 2 shows the final observed and calculated SXRD profiles for the Pb-doped sample.

For the SXRD refinement for the Pb-free sample, three phases are refined together. For the Hg-1223 phase, full occupation is assumed for all atoms except the partially occupied oxygen (O(4)) sited at the positions $(\frac{1}{2}, \frac{1}{2}, \frac{1}{2})$ of the Hg–O layer. The occupancy of O(4) is refined. To reduce the number of parameters needed in the refinements, three FWHM parameters, U, V, W, for all of the reflection lines of each phase are assumed as the same. Each phase is refined independently before they are refined together. During refinements, we find that if the occupancy of O(4) is varied from 0.30 to 0.36, there is no abnormal behaviour of any parameter. However, some of the isotropic thermal factors become negative if we set the occupancy of O(4) larger than 0.36. Also if we set some of the isotropic thermal factors to be zero, then the refined occupancy of O(4) is larger than 1.0. We conclude that the occupancy of O(4) in the Hg–O plane is less than 0.36. Full occupation is assumed for all atoms in $BaCuO_2$ and $CaHgO_2$ refinements. The refined structure parameters for the Pb-free sample are listed in table 2. Results of neutron powder diffraction refinements performed without splitting the Ba site [8] are also listed for comparison.

Table 2. Atomic parameters from SXRD refinements for pure Hg-1223 and for Pb-doped (Hg, Pb)-1223 samples. Results of neutron powder diffraction refinements for pure Hg-1223 [9] and for Pb-doped (Hg, Pb)-1223 [20] are also listed.

		Pure Hg-1223	Hg-1223 [9]	(Hg, Pb)-1223	(Hg, Pb)-1223 [20]
Hg (0, 0, $\frac{1}{2}$)	B (Å^2)	1.3(2)	3.9(2)	0.84(6)	0.02(2)
	Occupancy	1.0	1.0	0.62(7)	0.618(6)
Pb (0, 0, $\frac{1}{2}$)	B (Å^2)			0.9(2)	0.24(4)
	Occupancy			0.38	0.382
Ba ($\frac{1}{2}$, $\frac{1}{2}$, z)	z	0.3245(4)	0.3227(7)	0.3182(8)	0.3167(5)
	B (Å^2)	0.86(6)	2.2(3)	0.18(11)	2.12(8)
Ca ($\frac{1}{2}$, $\frac{1}{2}$, z)	z	0.1104(8)	0.1046(6)	0.0987(12)	0.0992(2)
	B (Å^2)	0.19(17)	0.0(2)	0.76(9)	0.13(5)
Cu(1) (0, 0, 0)	B (Å^2)	0.78(3)	1.2(2)	−0.0(2)	2.86(9)
Cu(2) (0, 0, z)	z	0.2004(5)	2021(4)	0.1990(7)	0.1998(4)
	B(Å^2)	1.47(10)	0.6(1)	1.5(4)	1.20(7)
O(1) ($\frac{1}{2}$, 0, 0)	B (Å^2)	1.52(24)	0.1(1)	1.52 (fixed)	1.52 (fixed)
O(2) ($\frac{1}{2}$, 0, z)	z	0.1966(23)	0.195(3)	0.194(2)	0.1928(3)
	B (Å^2)	0.30(27)	0.3(1)	0.30 (fixed)	0.30 (fixed)
O(3) (0, 0, z)	z	0.3823(65)	0.3764(5)	0.382(3)	0.3823(5)
	B (Å^2)	1.74(81)	0.9(2)	1.74 (fixed)	1.74 (fixed)
O(4) ($\frac{1}{2}$, $\frac{1}{2}$, $\frac{1}{2}$)	B (Å^2)	4.22(73)	1.2 (fixed)	4.22 (fixed)	4.22 (fixed)
	Occupancy	0.35 (fixed)	0.44(3)	0.46(6)	0.450(2)
a		3.8529(5)	3.8502(1)	3.84575(9)	3.8457(1)
c		15.8513(6)	15.7829(9)	15.8255(6)	15.8252(7)
R_p		12.14	6.44	11.97	10.98
R_{wp}		14.46	8.15	15.11	8.35
R_{exp}		6.37	4.95	4.36	3.33

For the optimally Pb-doped $Hg_{0.7}Pb_{0.3}Ba_2Ca_2Cu_3O_{8+\delta}$ (nominal composition) compound, the symmetry of the crystal structure is taken as that of the Pb-free compound. The initial parameters of each of the phases are taken from the above refinements. During the refinements, we find that the occupancy of Pb is strongly correlated with the thermal parameters of the oxygen atoms. To determine the actual Pb content, the thermal parameters of these atoms are fixed at the values obtained from the SXRD refinements for the pure Hg-1223 sample. The occupancy of Pb will be larger than 1.0 and the thermal parameters of oxygen will be negative if we allow the thermal parameters of oxygen to vary together. All other thermal parameters and atomic positions are allowed to vary, and show no abnormal behaviour. Like in the refinements for the pure Hg-1223, we have assumed full occupancy for ($Hg_{1-x}Pb_x$), and allow x and the partial oxygen content in the ($Hg_{1-x}Pb_x$)–O plane, δ, to vary. Some isotropic thermal factors will be less than zero if we fix $\delta < 0.40$. The impurity phases, $CaHgO_2$ and $BaCuO_2$, are contained in the ($Hg_{1-x}Pb_x$)-1223 samples. They are considered as the second and third phases in the refinement processes. The refined structure parameters for the Pb-doped sample are listed in table 2. Results of the neutron powder diffraction investigation for the Pb-doped sample [20] are also listed in table 2. Figure 2 shows the SXRD pattern with the calculated profile for Pb-doped Hg-1223.

The impurity phases exist in all samples and are refined. $CaHgO_2$ has an $R\bar{3}m$ symmetry

with $a = 3.584$ Å, 3.605 Å, and $c = 18.742$ Å, 19.054 Å for Pb-free and Pb-doped samples, respectively. The atomic positions are almost the same as those reported by Huang *et al* [10]. The $BaCuO_2$ phase has an $Im\bar{3}m$ symmetry with $a \sim 18.254$ Å and 17.741 Å for Pb-free and Pb-doped samples, respectively, which are smaller values than those in reference [23]. The atomic positions are also slightly different from those obtained by Weller and Lines [23].

The content of each phase can be obtained from the following formula [24]:

$$W_p = S_p(M\Omega)_p \Big/ \sum_j^3 S_j(M\Omega)_j$$

where we assume that all phases are refined for 100% of the specimen, j, p represent the jth and pth phases, M is the atomic weight of the formula unit, Ω is the volume of the unit cell, and S is the refined scale factor, which is obtained from

$$Y_{ci} = S_j \sum_k |F_K|^2 \Phi(\Delta 2\theta) L_K P_K + Y_{bi}.$$

Y_{ci} and Y_{bi} are the calculated and background intensities, respectively; F_K is the structure factor; $\Phi(\Delta 2\theta)$ is the reflection profile function; the Lorentz, polarization and multiplicity factors are contained in L_K; and P_K is the Rietveld–Toraya preferred-orientation function. From the refinements on the Pb-free sample, the scale factors are $(6.73 \pm 0.04) \times 10^{-4}$, $(2.43 \pm 0.26) \times 10^{-8}$ and $(4.05 \pm 0.07) \times 10^{-4}$ for the Hg-1223, $BaCuO_2$ and $CaHgO_2$ phases, respectively. The weight percentages are then calculated to be as follows: 70 wt% (Hg-1223), 17 wt% ($BaCuO_2$) and 13 wt% ($CaHgO_2$), respectively. For the Pb-doped sample ($x = 0.30$), the scale factors are $(3.41 \pm 0.02) \times 10^{-4}$, $(1.84 \pm 0.17) \times 10^{-8}$ and $(6.67 \pm 0.08) \times 10^{-4}$ for the Hg-1223, $BaCuO_2$ and $CaHgO_2$ phases, respectively. The weight percentages are then calculated to be as follows: 54 wt% (Hg-1223), 17 wt% ($BaCuO_2$) and 29 wt% ($CaHgO_2$), respectively.

When comparing the above refinements to the neutron powder diffraction refinements (see table 2), we find that larger errors appear in the SXRD refinements, especially for the oxygen parameters. The atomic coordinations for the heavy atoms, such as Hg, Pb, Ba, in the superconducting phase obtained by SXRD refinements are almost the same as those obtained by NPD refinements. The difference between the atomic parameters obtained in this work and by Chmaissem *et al* [8] may be due to the difference between the synthesis procedures. One reason is the weak x-ray scattering power of the oxygen atoms. Another probable reason is that there are too many variable parameters in our refinements. The neutron powder diffraction refinement results are also listed in table 2.

Comparing Pb-doped ($Hg_{1-x}Pb_x$)-1223 ($x = 0.30$) to Pb-free Hg-1223, we note that Pb partially replaces Hg, and the occupancy of oxygen sited in the Hg(Pb)–O plane, O(4), increases to nearly a half for full occupation ($\delta = 0.46(6)$) for the Pb-doped sample ($x = 0.3$). These findings are consistent with the notion that substitution of Pb for Hg in the 1223 compound stabilizes the necessary fractional oxygen content, and thereby raises T_c. The partial Pb concentration obtained by the refinement is about 26% larger than that of the starting stoichiometry. This discrepancy may arise because some amounts of HgO, CaO, BaO and CuO form other impurities, e.g. $CaHgO_2$ and $BaCuO_2$ during, calcination, and because of the reduction in the amount of Hg required to form (Hg, Pb)-1223. Similar results are obtained in the Tl-doped $Hg_{0.80}Tl_{0.20}Ba_2Ca_2Cu_3O_{8+d}$ system [18]. For the Tl-doped Hg-1223 sample, the refined content of Tl is almost double the nominal value, but the impurities contained in the Tl-doped sample are $CaHgO_2$ and $Ca_{0.85}CuO_2$ and some unknown impurity phases.

Table 3. Selected bond distances from SXRD refinements. Corresponding distances for Tl-doped Hg-1223 [18] are also listed.

Bond	Cu(1)–O(1)	Cu(2)–O(2)	Cu(2)–O(3)	Hg–O(3)	Hg–O(4)
Pure Hg-1223	1.9264(1)	1.927(22)	2.883(4)	1.866(11)	2.7244(2)
(Hg, Pb)-1223	1.922 88(2)	1.924(18)	2.896(22)	1.786(19)	2.719 36(3)
(Hg, Tl)-1223	1.924 45(3)	1.924(11)	2.853(9)	1.796(7)	2.721 58(4)

The lattice parameters of the Pb-doped (Hg, Pb)-1223 sample are slightly less than those of the pure Hg-1223 sample, with $\mathrm{d}a/\mathrm{d}T_c = -3.6 \times 10^{-4}$ Å K^{-1} and $\mathrm{d}c/\mathrm{d}T_c = -1.3 \times 10^{-3}$ Å K^{-1}. To compare these values quantitatively to the pressure-induced lattice parameter change, we note that the rate of increase of T_c with pressure for pure Hg-1223 is about 1.7 K GPa^{-1}, and that the compressibilities along the a- and c-axes are $\kappa_a = 2.28 \times 10^{-3}$ GPa^{-1} and $\kappa_c = 4.7 \times 10^{-3}$ GPa^{-1}, respectively [10]. From these data, we estimate that the pressure-induced change in T_c will exhibit lattice parameter changes of $\mathrm{d}c/\mathrm{d}T_c = -4.4 \times 10^{-2}$ Å K^{-1}, and $\mathrm{d}a/\mathrm{d}T_c = -5.09 \times 10^{-3}$ Å K^{-1}. These values are an order of magnitude larger than those deduced for Pb-substituted samples. Therefore, the lattice parameter contraction due to partial substitution of Pb for Hg is not sufficient to account for the observed change in T_c. The change in T_c may be due to the change of the carrier concentration for the Pb-doped sample.

Table 3 also lists several selected bond distances for pure Hg-1223, Pb-doped Hg-1223 and Tl-doped Hg-1223 [18] at room temperature. For the pure Hg-1223 compound, the in-plane Cu–O bond distance is almost identical for the two different kinds of (CuO_2) layer. A comparison with other members of the homologous series shows that this bond length is strongly dependent on the oxidation state of copper, varies from compound to compound, and changes with the oxygen content in the same compound. Thus if we consider the compositions corresponding to the optimum value of T_c in each case, this separation is about 1.942 Å in Hg-1201 [3], 1.926 Å in Hg-1212 [4] and 1.926 Å in Hg-1223 (this work), i.e. it decreases with increasing oxidation of the copper atoms. The same behaviour is observed for different oxygen contents in the same compound. In Hg-1212, the in-plane Cu–O separation is 1.9263(1) Å and 1.972(1) Å for $\delta = 0.35$ and 0.28, respectively [4], and 1.9290 Å for $\delta = 0.22$ [11]. The apical Cu–O distance, involving the copper atoms with pyramidal coordination, is very large (2.883 Å) when compared to the values for other layered copper oxide superconductors. Typical values are 2.32 Å for YBCO [25] and 2.41 Å for LSCO [26]. For the Pb-doped (Hg, Pb)-1223 sample, the in-plane Cu–O bond distance is not the same, the Cu(1)–O(1) bond distance (1.9228 Å) is smaller than that of Cu(2)–O(2) (1.926 Å), and also smaller than that for the pure Hg-1223 sample. The apical Cu(2)–O(3) bond distance (3.076 Å) is much larger than that for the pure Hg-1223 sample. On the other hand, the (Hg/Pb)–O(3) bond distance for the Pb-doped sample (1.785(7) Å) is smaller than that for the pure sample (1.866(4) Å), but the (Hg/Pb)–O(4) bond distances are almost the same for those two samples. From these differences, we deduce that the increase of T_c may also be related to three kinds of bond distance: the in-plane Cu(2)–O(2), the apical Cu(2)–O(3), and the two fold dumbbell Hg–O(3).

That the bond distance of (Hg/Pb)–O(3) in the Pb-doped sample is shorter than that of Hg–O(3) in the Pb-free sample is also proved from the Raman measurement. Raman spectra of $Hg_{0.7}Pb_{0.3}Ba_2Ca_2Cu_3O_{8+\delta}$ for different laser irradiation powers are shown in figure 3. Eight peaks at the frequencies of 107 cm^{-1}, 116 cm^{-1}, 232 cm^{-1}, 477 cm^{-1}, 578 cm^{-1}, 597 cm^{-1}, 632 cm^{-1} and 671 cm^{-1} are observed. The 590 cm^{-1} band is assigned to the

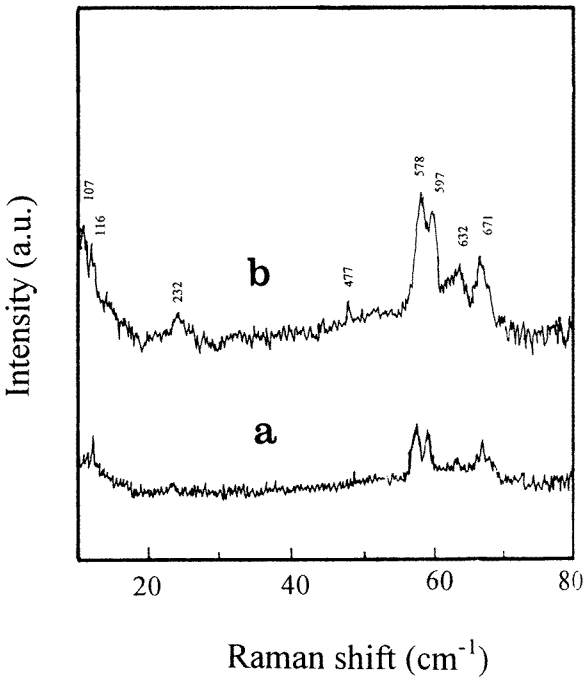

Figure 3. Raman spectra of $Hg_{0.7}Pb_{0.3}Ba_2Ca_2Cu_3O_{8.46}$ at room temperature for different laser irradiation powers: (a) 100 μW; (b) 250 μW.

O(3) A_{1g} mode by Yang *et al* [13], Ren *et al* [14] and Chang *et al* [15]. The Raman peak appearing at 597 cm^{-1} for the Pb-doped sample is higher than that appearing at 585 cm^{-1} [13] and 586 cm^{-1} [15]. This result indicates that the (Hg/Pb)–O(3) bond distance in the Pb-doped sample is less than that in the Pb-free sample. The peak at 578 cm^{-1} for the Pb-doped sample is just the same as those obtained by Yang *et al* [13] (574 cm^{-1}) and by Chang *et al* [15] (576 cm^{-1}) for pure Hg-1223. This peak can be attributed to the motion of the O(4) (oxygen in (HgO_δ)) E_u mode [1]. However, Yang *et al* [13] assigned this peak to the O(2) A_{1g} mode. The peak at 107 cm^{-1} is observed at high laser radiation power. The Ba–O bond length in (Hg, Pb)-1223 is longer than that in pure Hg-1223. Yang *et al* [13] assigned a peak at 92 cm^{-1} to the Ba A_{1g} mode. This peak may correspond a Ba A_{1g} mode or an impurity peak. The peak at the frequency of 477 cm^{-1} is similar to the peak in pure Hg-1223 [13] (479 cm^{-1}), which is assigned to O(3) E_g mode. The peak at 116 cm^{-1} is the Ar^+ plasma line of the laser beam. The Raman peaks at 232 cm^{-1} and 671 cm^{-1} are due to the $CaHgO_2$ [13]. The peak at the frequency of 632 cm^{-1} is due to the $BaCuO_2$ phase [13]. The Raman peak positions are not shifted when the laser irradiation power is changed (see figure 3).

4. Conclusion

In summary, Hg in the Hg-1223 superconductor can be partially substituted for with Pb, resulting in an increase of T_c. Moreover, the lattice parameters a and c decrease with the increase of the Pb content. The changes in lattice parameters caused by such a chemical

substitution are too weak to account for the change in T_c by mimicking the effect of pressure. The Raman spectra are also measured for the Pb-doped sample. The spectrum shows peaks at 578 cm^{-1} and 597 cm^{-1}, which proves the subtlety of the structure change due to the Pb doping of the Hg-1223 superconductor.

References

[1] Putilin S N, Antipov E V, Chmaissem O and Marezio M 1993 *Nature* **362** 226
[2] Schilling A, Cantoni M, Guo J D and Ott H R 1993 *Nature* **363** 56
[3] Chmaissem O, Huang Q, Putilin S N, Marezio M and Santoro A 1993 *Physica* C **212** 259
[4] Antipov E V, Capponi J J, Chaillout C, Chmaissem O, Loureiro S M, Marezio M, Putilin S N, Santoro A and Tholence J L 1993 *Physica* C **218** 348
[5] Meng R L, Beauvais L, Zhang X N, Huang Z J, Sun Y Y, Xue Y Y and Chu C W 1993 *Physica* C **216** 21
[6] Nunez-Regueiro M, Tholence J, Antipov E V, Capponi J and Marezio M 1993 *Science* **262** 97
[7] Antipov E V, Putilin S N, Kopnin E M, Capponi J J, Chaillout C, Loureiro S M, Marezio M and Santoro A 1994 *Physica* C **235–240** 21
[8] Chmaissem O, Huang Q, Antipov E V, Putilin S N, Marezio M, Loureiro S M, Capponi J J, Tholence J L and Santoro A 1993 *Physica* C **217** 265
[9] Hunter B A, Jorgensen J D, Wagner J L, Raedelli P G, Hinks D G, Shaked H, Hitterman R L and Von Dreele R B 1994 *Physica* C **221** 1
[10] Huang Q, Lynn J W, Meng R L and Chu C W 1993 *Physica* C **218** 356
[11] Loureiro S M, Antipov E V, Tholence J L, Capponi J J, Chmaissem O, Huang Q and Marezio M 1993 *Physica* C **217** 253
[12] Wu X S, Shao H M, Jiang S S, and Yao X X 1995 *Phys. Status Solidi* a **152** 477
[13] Yang In-Sang, Lee Hye-Gyong, Shin Hye-Soo and Park Jung-Hae 1994 *Physica* C **222** 386
[14] Ren Y T, Chang H, Xiong Q, Wang Y Q, Sun Y Y, Meng R L, Xue Y Y and Chu C W 1993 *Physica* C **217** 273
[15] Chang H, He Z H, Meng R L, Xue Y Y and Chu C W 1995 *Physica* C **251** 126
[16] Isawa K, Tokiwa-Yamamoto A, Itoh M and Yamauchi S A 1994 *Physica* C **222** 33
[17] Hur N H, Kim N H, Lee K W and Park Y K 1994 *Mater. Res. Bull.* **29** 959
[18] Dai P, Chakoumakos B C, Sun G F, Wong K W, Xin Y and Lu D F 1995 *Physica* C **243** 201
[19] Shao H M, Lam C C, Fung P C W, Wu X S, Du J H, Shen G J, Chow J C L, Ho S L, Hung K C and Yao X X 1995 *Physica* C **246** 207
[20] Wu X S, Gou C, Chen D F, Shao H M, and Jiang S S 1996 *J. Phys.: Condens. Matter* **8** 3647
[21] Shao H M, Shen L J, Shen J C, Hua X Y, Yuan P F and Yao X X 1994 *Physica* C **232** 5
[22] Izumi F 1985 *Kobutsugaku Zasshi* **17** 37
[23] Weller M T and Lines D R 1987 *J. Solid State Chem.* **82** 21
[24] Hill R J and Howard L J 1987 *J. Appl. Crystallogr.* **20** 467
[25] Beech F, Miraglia S, Santoro A and Roth R S 1987 *Phys. Rev.* B **35** 8778
[26] Cava R J, Santoro A, Johnston D W and Rhodes W W 1987 *Phys. Rev.* B **35** 6716